

Developmental Cell 18

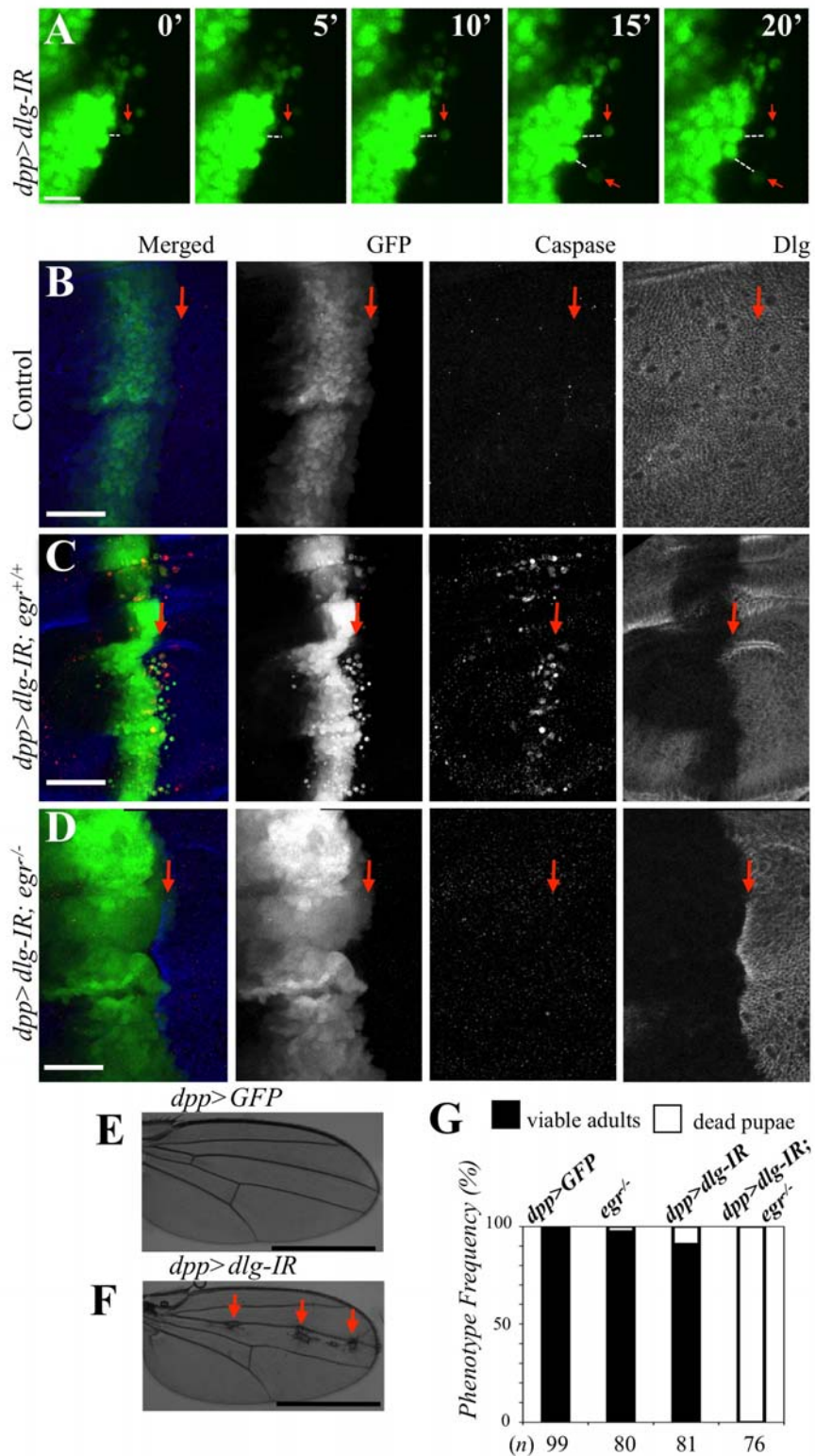
Supplemental Information

Oncogenic Ras Diverts a Host

TNF Tumor Suppressor Activity

into Tumor Promoter

**Julia B. Cordero, Juan P. Macagno, Rhoda K. Stefanatos, Karen E. Strathdee,
Ross L. Cagan, and Marcos Vidal**



Cordero et al, Fig. S1

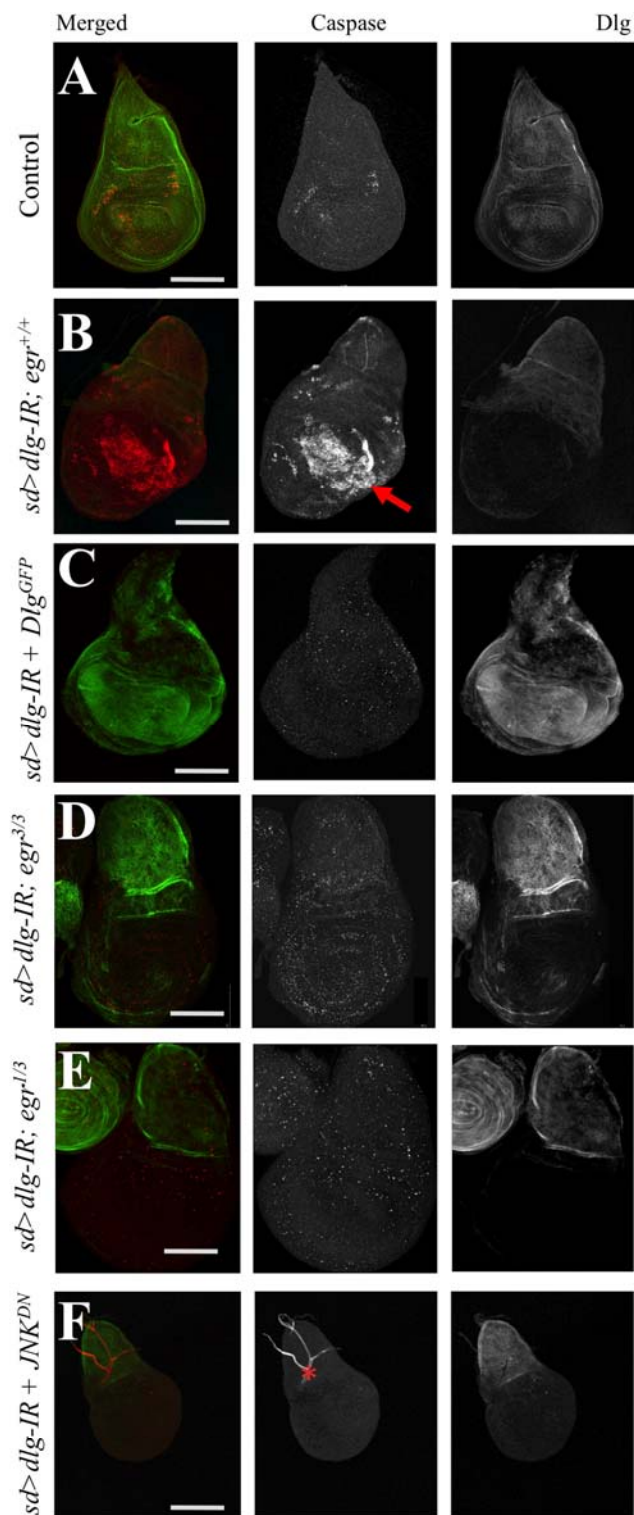
Figure S1, Related to Figure 1. *dlg*-deficient cell delamination and apoptosis are *egr*-dependent

A, Snapshots taken every 5 minutes from a live-visualization experiment using a *dpp>dlg-IR+GFP* wing disc. Arrows point to cells that displace away from the bulk of GFP cells. Dotted lines trace the distance travelled by migrating cells. Scale bar: 10 μ m.

B-D, Confocal projections from larval wing discs. Panels in the left column are color overlays from GFP (green), cleaved Caspase-3 (red) and Dlg (blue) fluorescent

signals; the remaining columns show individual stains in gray for additional clarity. Arrows indicate anterior/posterior (A/P) boundary; the *dpp* expression domain is an anterior stripe at the boundary. Scale bars: 150 μ m. **E, F**, adult wings from *dpp>GFP* (control, **E**) and *dpp>dlg-IR+GFP* (**F**). Arrows indicate scars observed along the A/P axis. Scale bars: 1 mm. **G**, Quantification of phenotype frequencies. The relevant genotypes are indicated on top of each column, and the number of animals counted at the bottom. Note that while most animals from control genotypes and *dpp>dlg-IR+GFP* (91%, n=81) reached adulthood, *dpp>dlg-IR+GFP; egr^{-/-}* died as pupae (100%, n=76).

Genotypes: **A, C, F**, *w/w; dpp-gal4, UAS-GFP^{NLS}/UAS-dlg-IR^{VDRC41136}*. **B, E**, *w/w; dpp-gal4, UAS-GFP^{NLS}*. **D**, *w/w; egr³/egr³; dpp-gal4, UAS-GFP^{NLS}/UAS-dlg-IR^{VDRC41136}*. **G**, 1st column: *w/w*. 2nd column: *w/w; egr³/egr³*. 3rd column: *w/w; dpp-gal4, UAS-GFP^{NLS}/UAS-dlg-IR^{VDRC41136}*. 4th column: *w/w; egr³/egr³; dpp-gal4, UAS-GFP^{NLS}/UAS-dlg-IR^{VDRC41136}*.

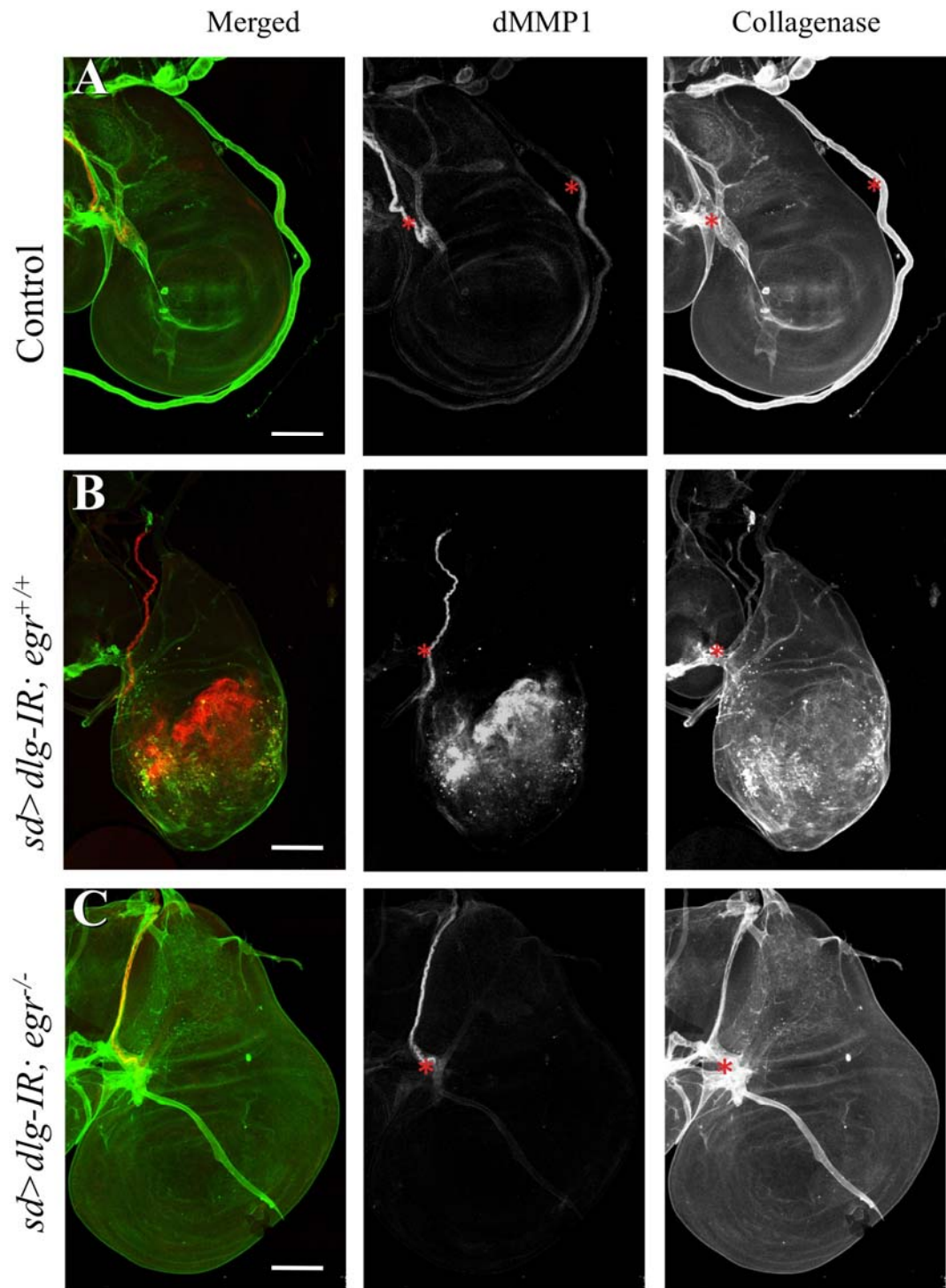


Cordero et al, Fig. S2

Figure S2, Related to Figure S1. JNK- and *egr*-dependency on *dlg-IR* cell apoptosis

Confocal projections from larval wing discs. Left panels: overlays of cleaved Caspase-3 (red) and Dlg (green) immunofluorescent antibody staining. Each signal is also displayed individually in grayscale as labeled. The arrow in **B** points to foci of apoptotic cell death within the *sd* expression domain at the wing pouch (ventral) region of the wing discs. The asterisk marks overlaying trachea branches. Scale bars: 150 μ m.

Genotypes: **A**, *w, sd-gal4/w*. **B**, *w, sd-gal4/w; UAS-dlg-IR^{VDRC41136}*. **C**, *w, sd-gal4/w; UAS-dlg-IR^{VDRC41136}/UAS-Dlg^{GFP}*. **D**, *w, sd-gal4/w; , egr³/egr³; UAS-dlg-IR^{VDRC41136}*. **E**, *w, sd-gal4/w; , egr¹/egr³; UAS-dlg-IR^{VDRC41136}*. **F**, *w, sd-gal4/w, UAS-bsk^{DN}; UAS-dlg-IR^{VDRC41136}*.



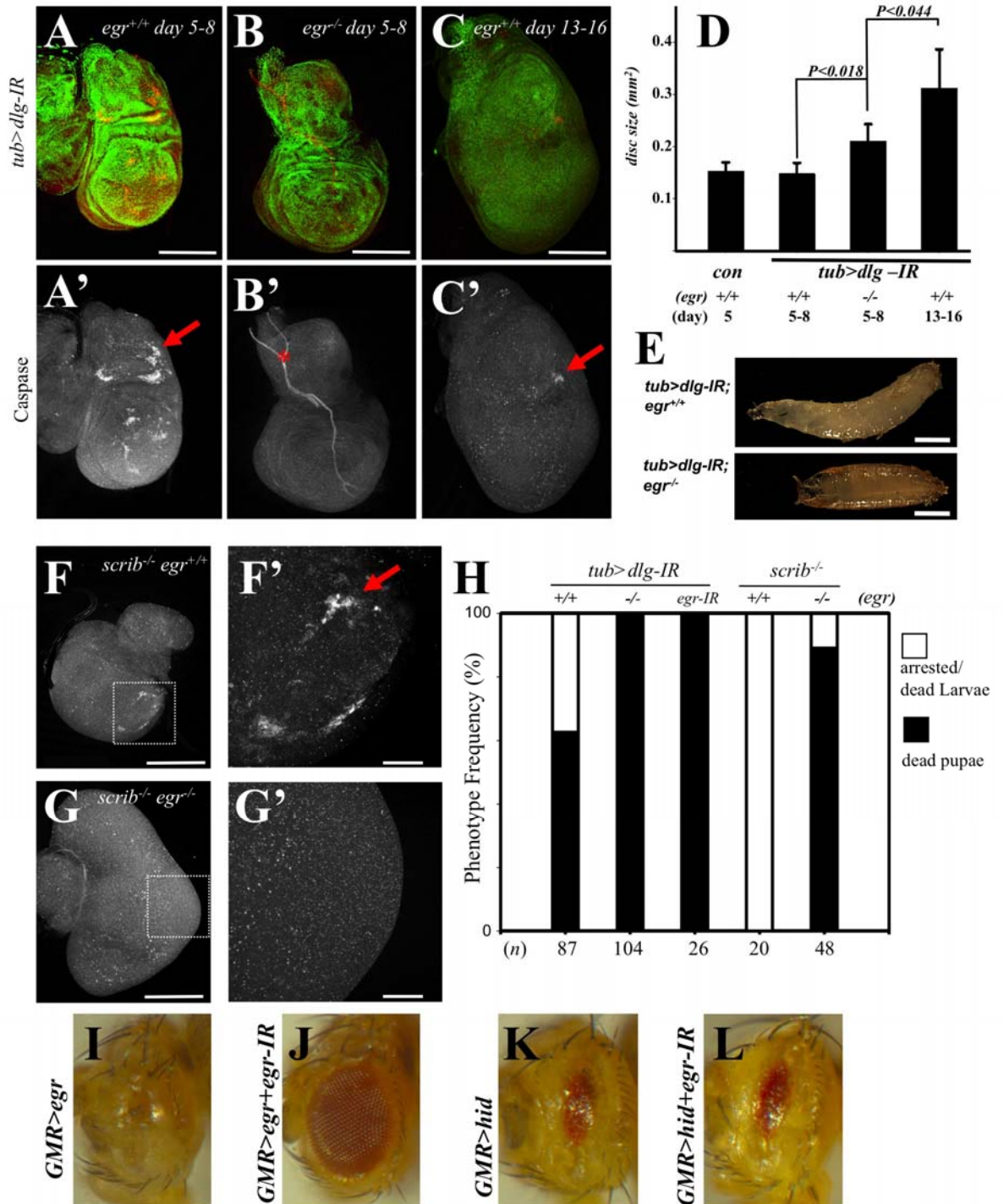
Cordero et al, Fig. S3

Figure S3, Related to Figure 1. Extracellular Matrix remodeling and dMMP1 expression in *dlg* cells

Confocal images of larval wing discs from animals with the indicated relevant genotypes, stained for dMMP1 (red and centre column) and Collagenase/Gelatinase

activity to visualize MMP activity *in situ* (green and right column). Scale bars: 100 μ m. Asterisks label overlaying trachea branches, known to express dMMP1. Note that reducing Dlg levels in the wing pouch resulted in a drastic up-regulation of dMMP1 and increased foci of Collagenase/Gelatinase activity *in situ*. Such phenotypes were fully dependent on *egr*.

Genotypes: **A**, *w, sd-gal4/w*; **B**, *w, sd-gal4/w; UAS-dlg-IR^{VDR41136}*. **C**, *w, sd-gal4/w; egr³/egr³; UAS-dlg-IR^{VDR41136}*.



Cordero et al, Fig. S4

Figure S4, Related to Figure 2. A role for *egr* in the ubiquitous loss of *dlg* and *scrib*

A-C, Larval wing discs from *tub>GFP+dlg-IR* animals. The indicated *egr* background and age range (in days after embryo deposition) are indicated. Top panels show an overlay from nuclei (green) and cleaved Caspase-3 (red); the latter stain is shown in gray in the lower panels. Arrows point to foci of cleaved Caspase staining. Asterisks mark overlaying tracheal branches. Scale bars: 200 μ m.

D, Quantification of *tub>dlg-IR+GFP* wing disc sizes. The *P* value in a two-tailed student's *t*-test is displayed ($n=4$, error bars are s.e.m.).

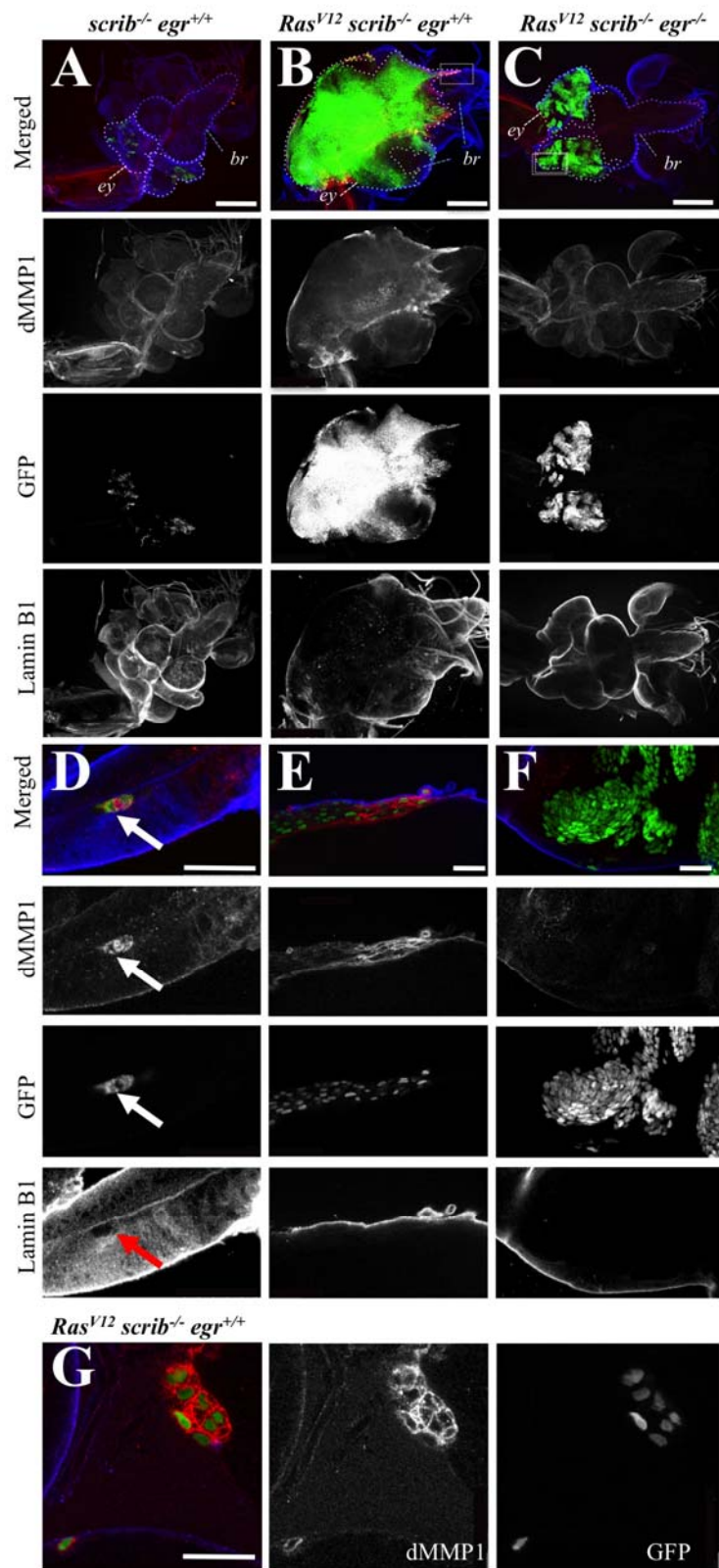
E, Micrographs from animals with the indicated genotypes. Scale bars: 750 μ m.

F, G, Wing discs from *scrib^{-/-}; egr^{+/+}* (**F**) and *scrib^{-/-}; egr^{-/-}* (**G**) animals, stained for cleaved Caspase-3. Panels in the right show high magnification views from the boxed areas. Scale bars: 250 μ m (F, G) and 50 μ m (F', G').

H, Phenotype frequencies for the relevant genotypes indicated on top of each column. The number of animals counted is displayed at the bottom. Note that in both *tub>dlg-IR* and *scrib^{-/-}* animals, the absence of *egr* suppressed the developmental arrest at the larval stage from 37% to 0% for *tub>dlg-IR* ($n=87$ for *egr^{+/+}*, $n=104$ for *egr^{-/-}* and $n=26$ for *egr-IR*) and from 100% to 10.5% for *scrib^{-/-}* ($n=20$ for *egr^{+/+}* and $n=48$ for *egr^{-/-}*).

I-L, Rescue of *egr*-misexpression by *egr-IR*. Adult eye micrographs are shown from animals with the following relevant genotypes: **I**, *GMR>egr*. **J**, *GMR>egr+egr-IR*. **K**, *GMR>hid*. **L**, *GMR>hid+egr-IR*. Note that *egr* mis-expression with the *GMR* promoter resulted in an ablated-eye phenotype. This phenotype was fully rescued by the *egr* RNAi transgene (*egr-IR*). Such rescue was not due to general anti-apoptotic effects since *egr-IR* failed to modify the phenotype resulting from mis-expression of the pro-apoptotic gene *hid*.

Full Genotypes: **A, C**, 2nd and 4th column in **D, E** (top), and first column in **H**: *yw, tub-gal4, UAS-GFP^{NLS}; UAS-dlg-IR^{VDRC41136}*. **B**, 3rd column in **D, E** (bottom) and 2nd column in **H**: *yw, tub-gal4, UAS-GFP^{NLS}; egr³/egr³; UAS-dlg-IR^{VDRC41136}*. 3rd column in **H**: *yw, tub-gal4, UAS-GFP^{NLS}; UAS-dlg-IR^{VDRC41136}/UAS-egr-IR^{VDRC42252}*. **F** and 4th column in **H**: *w; FRT^{82B}, scrib¹/FRT^{82B}, scrib¹*. **G** and 5th column in **H**: *w; egr³/egr³; FRT^{82B}, scrib¹/FRT^{82B}, scrib¹*. **I**, *w, GMR-gal4/w; UAS-egr*. **J**, *w, GMR-gal4/w; UAS-egr; UAS-egr-IR^{VDRC42252}*. **K**, *w, GMR-gal4/w; GMR-hid*. **L**, *w, GMR-gal4/w; GMR-hid; UAS-egr-IR^{VDRC42252}*.

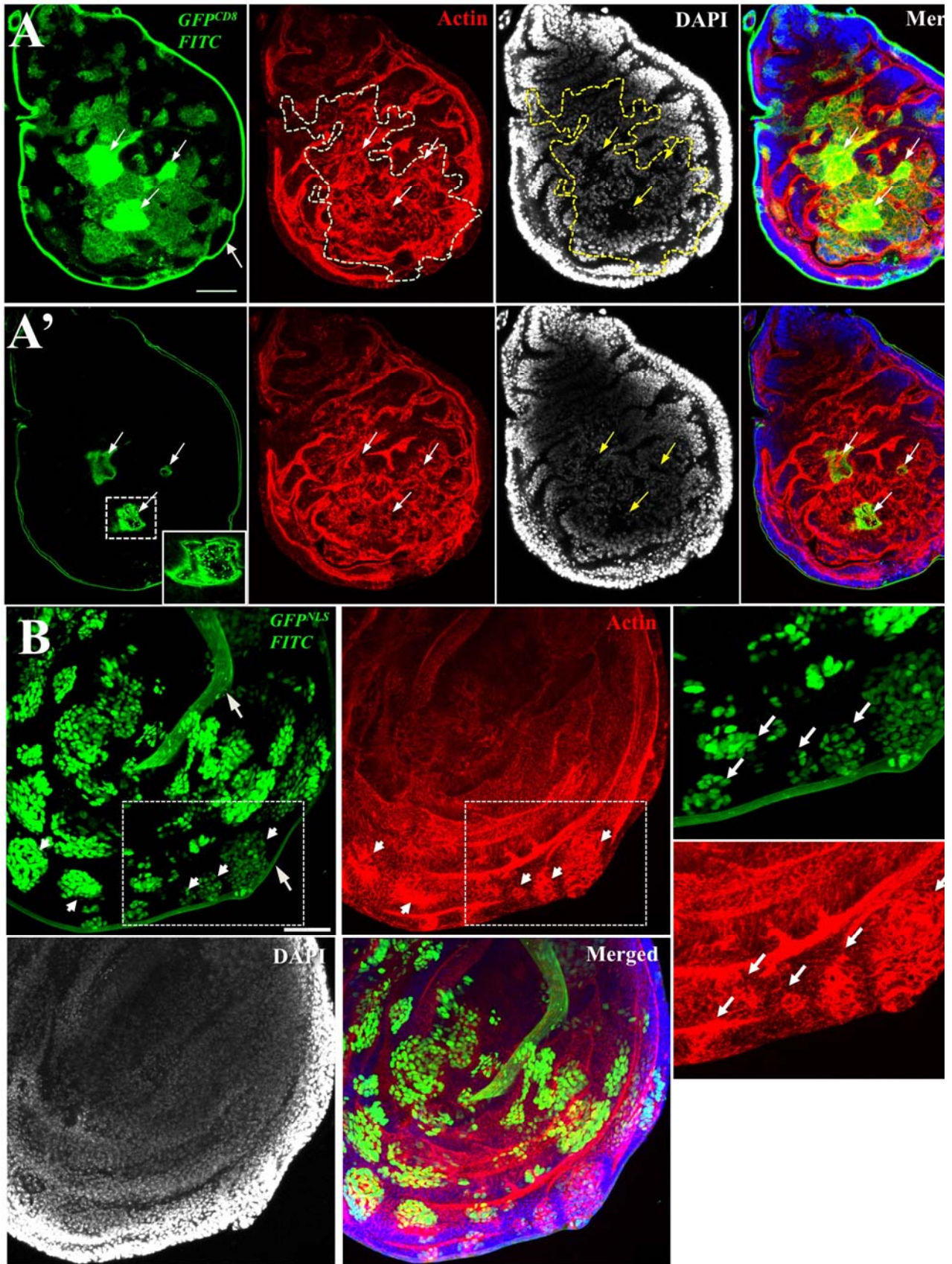


Cordero et al, Fig S5

Figure S5, Related to Figure 2. Additional data on the interaction between *Ras^{V12}*, *scrib* and *Egr*

A-F, Expansion from Figure 2 displaying individual stains in grey from the merged panels, as indicated. The phenotype of *scrib^{-/-}* clones is also shown. GFP-labeled clones of cells with the genotypes stated below were created in developing eye-antennae discs. Confocal images from larval cephalic complexes labeled for GFP (green), dMMP1 (red) and Laminin B1 (blue). The arrow in **D** points to a single-cell *scrib* mutant clone displaying dMMP1 expression and degradation of the underlying

ECM. **G**, Early, small clones of Ras^{V12} ; $scrib^{-/-}$ displayed high levels of dMMP1 through the clones. Scale bars: 200 μm (**A-C**), 25 μm (**D-G**).
 Genotypes: **A, D**, $yw, tub-gal4, UAS-GFP^{NLS}/yw, ey(3.5)FLP; FRT^{82B}, scrib^1/FRT^{82B}, tub-gal80$. **B, E, G**, $yw, tub-gal4, UAS-GFP^{NLS}/yw, ey(3.5)FLP; UAS-Ras^{V12}; FRT^{82B}, scrib^1/FRT^{82B}, tub-gal80$. **C, F**, $yw, tub-gal4, UAS-GFP^{NLS}/yw, ey(3.5)FLP; UAS-Ras^{V12}, egr^3/egr^3; FRT^{82B}, scrib^1/FRT^{82B}, tub-gal80$.

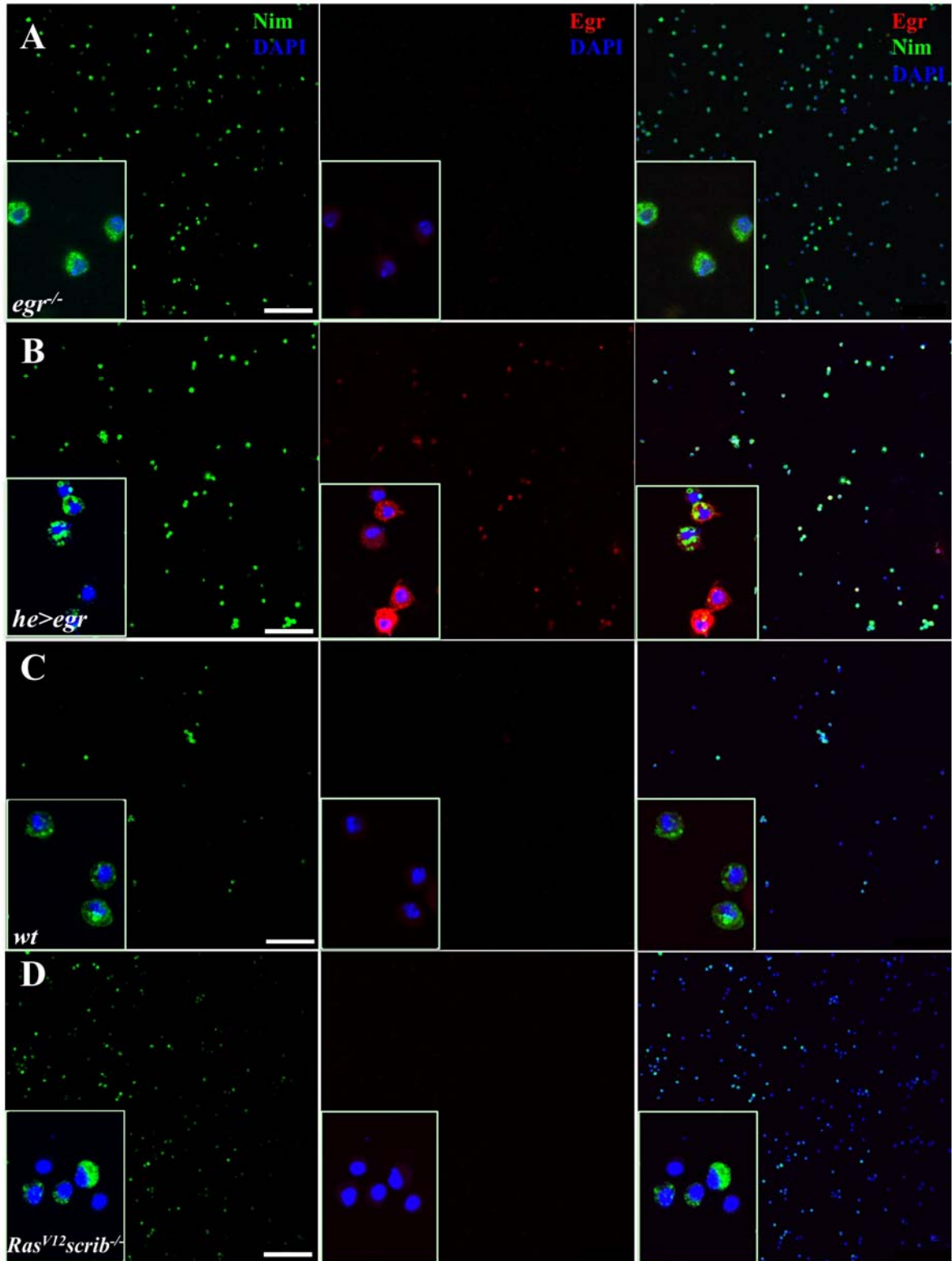


Cordero et al, Fig S6

Figure S6, Related to Figure 2. Ras^{V12} , $scrib$ clones in the wing disc

GFP-labeled clones of *Ras*^{V12}, *scrib* cells were created in the wing discs of *egr*⁺ (**A**) and *egr*^{-/-} animals (**B**). The tissues were stained for Collagenase activity (FITC-green), Actin fibers (Red) and DAPI (blue). The merged images and individual stains are shown as labeled. Note that the fluorescence spectra from FITC (Collagenase activity) and GFP (clones) overlapped. However, the signals could be resolved based on their localization (membrane associated CD8-GFP in **A** and nuclear GFP in **B**; extracellular localization for FITC-Collagenase activity). Note the basal membrane staining for Collagenase activity as the outline of the tissue. In **A**, numerous foci of ectopic Collagenase activity were observed (arrows). **A'** shows a confocal plane from the projection in **A** that did not include the clonal cell bodies. The inset shows a high magnification view from the boxed area displaying foci typical of ectopic Collagenase activity (e.g; Figure 1G). **B**, Ectopic Collagenase activity was absent in the *egr*^{-/-} background, which displayed only the normal Collagenase activity at the basal membrane (arrows in **B**; Fig. 1F). The abnormal remodeling of Actin fibers was observed irrespectively of *egr* (e.g.; arrowheads in **B**). The two right panels show magnified views of the boxed areas in B. Scale bars: 40 μm.

Genotypes: **A**, *yw*, *hs-FLP*, *UAS-CD8-GFP*; *tub-gal4/UAS-Ras*^{V12}; *FRT*^{82B}, *scrib*¹/*FRT*^{82B}, *tub-gal80*. **B**, *yw*, *hs-FLP*, *tub-gal4,UAS-GFP*^{NLS}; *UAS-Ras*^{V12}, *egr*³/*egr*³; *FRT*^{82B}, *scrib*¹/*FRT*^{82B}, *tub-gal80*.



Cordero et al, Fig S7

Figure S7, Related to Figure 3. Circulating haemocytes do not express Eiger
 Haemolymph cells were stained for Nimrod C1 (Green), Eiger (Red) and DAPI (Blue) from larvae with the indicated genotypes. The insets show high magnification views. Note that both in the case of haemolymph from wild type (C) or from animals bearing $Ras^{V12}; scrib^{-/-}$ tumors (D), the staining for Eiger was a weak signal indistinguishable from *egr* mutants (A). High levels of Eiger were observed when Eiger was forcedly expressed in haemocytes (B). Scale bars: 100 μ m.
 Genotypes: **A**, *w; egr³/egr³*. **B**, *w; UAS-Eiger/hemese-gal4*. **C**, *w*, **D**, *yw, ey(3.5)FLP; act>y⁺>gal4, UAS-GFP/ UAS-Ras^{V12}; FRT^{82B}, scrib¹/FRT^{82B}, tub-gal80*.

SUPPLEMENTAL EXPERIMENTAL PROCEDURES

RNAi transgene validation: For *UAS-egr-IR^{VDRC42252}* (*egr-IR*), we co-expressed it in the developing eye together with *UAS-egr*. The ablated eye phenotype of *GMR>egr* was fully rescued by *egr-IR* (Fig. S5). For *UAS-dlg-IR^{VDRC41136}* (*dlg-IR*), we observed that (i) phenocopied *dlg* mutant alleles when ubiquitously expressed (Fig. 3C, E) and (ii) decreased levels of the Dlg protein as judged by immunofluorescence (Fig S1 and S2). Genotyping *egr* mutants: during the generation of new genotypes, the presence of the *egr³* mutant allele was assessed by PCR from genomic DNA with the primers GTTTTCGCGCTTTTCTTTTG and ATCGAGCTTTGTCGCACTTT.

Full genotypes for main Figures:

Figure 1:

A, *w/w; dpp-gal4, UAS-GFP^{NLS}/UAS-dlg-IR^{VDRC41136}*. **B**, *w/w; egr³/egr³; dpp-gal4, UAS-GFP^{NLS}/UAS-dlg-IR^{VDRC41136}*. **C, F**, *w, sd-gal4/w*. **D, G**, *w, sd-gal4/w; UAS-dlg-IR^{VDRC41136}*. **E, H**, *w, sd-gal4/w; egr³/egr³; UAS-dlg-IR^{VDRC41136}*.

Figure 2:

A, C, E, G, 3rd column in **I**, *yw, tub-gal4, UAS-GFP^{NLS}/yw,ey(3.5)FLP; UAS-Ras^{V12}; FRT^{82B}, scrib¹/FRT^{82B}, tub-gal80*. **B, D, F, H**, 4th column in **I**, *yw, tub-gal4, UAS-GFP^{NLS}/yw, ey(3.5)FLP; UAS-Ras^{V12}, egr³/egr³; FRT^{82B}, scrib¹/FRT^{82B}, tub-gal80*.

1st column in **I**, *yw, tub-gal4, UAS-GFP^{NLS}/yw,ey(3.5)FLP; FRT^{82B}, scrib¹/FRT^{82B}, tub-gal80*. 2nd column in **I**, *yw, tub-gal4, UAS-GFP^{NLS}/yw,ey(3.5)FLP; egr³/egr³; FRT^{82B}, scrib¹/FRT^{82B}, tub-gal80*.

Figure 3:

All panels except **C**: *yw,ey(3.5)FLP; act>y⁺>gal4, UAS-GFP/ UAS-Ras^{V12}; FRT^{82B}, scrib¹/FRT^{82B}, tub-gal80*. **C**, *yw, tub-gal4, UAS-GFP^{NLS}/yw,ey(3.5)FLP; UAS-Ras^{V12}, egr³/egr³; FRT^{82B}, scrib¹/FRT^{82B}, tub-gal80*.

Figure 4:

A, *yw,hs-FLP, UAS-CD8-GFP; lgl⁴, FRT^{40A}/ tub-gal80, FRT^{40A}; tub-gal4*. **B**, *w¹¹¹⁸*. **C**, first box in **E**, *w, sd-gal4/w*. **D**, second box in **E**, *w, sd-gal4/w; UAS-dlg-IR^{VDRC41136}*.

Figure 5:

In **C-D**, the haemolymph donors were: *w; UAS-RFP^{NLS}; hemese-gal4*. Acceptors: **C**, *yw,ey(3.5)FLP; act>y⁺>gal4, UAS-GFP; FRT^{82B}/FRT^{82B}, tub-gal80*. **D**, *yw,ey(3.5)FLP; act>y⁺>gal4, UAS-GFP/ UAS-Ras^{V12}; FRT^{82B}/FRT^{82B}, tub-gal80*. **E** and **G**, *yw,ey(3.5)FLP; act>y⁺>gal4, UAS-GFP; FRT^{82B}, scrib¹/FRT^{82B}, tub-gal80*. **F**, *yw,ey(3.5)FLP; act>y⁺>gal4, UAS-GFP/ UAS-Ras^{V12}; FRT^{82B}, scrib¹/FRT^{82B}, tub-gal80*.

Figure 6:

A, *yw,hs-FLP/UAS-dicer; lgl⁴, FRT^{40A}/ubi-GFP^{NLS}, FRT^{40A}; TM6b/ UAS-egr-IR^{VDRC42252}*. **B** and **C**, *yw,hs-FLP/UAS-dicer; lgl⁴, FRT^{40A}/ubi-GFP^{NLS}, FRT^{40A}; hemese-gal4/ UAS-egr-IR^{VDRC42252}*.

D, *yw,ey(3.5)FLP/UAS-dicer; lgl⁴, FRT^{40A}/ubi-GFP^{NLS}, FRT^{40A}; TM6b/ UAS-egr-IR^{VDRC42252}*. **E**, *yw,ey(3.5)FLP/UAS-dicer; lgl⁴, FRT^{40A}/ubi-GFP^{NLS}, FRT^{40A}; hemese-gal4/ UAS-egr-IR^{VDRC42252}*.

Figure 7:

A, *w; FRT^{82B}, scrib¹/ FRT^{82B}, scrib¹*. **B-D**, *w; egr³/egr³; FRT^{82B}, scrib¹/ FRT^{82B}, scrib¹*. In **C**, the haemolymph donors were *w*, while in **D**, they were *w; egr³/egr³*.

In **E-H**, the haemolymph acceptors were: *yw, tub-gal4, UAS-GFP^{NLS}/yw, ey(3.5)FLP*; *UAS-Ras^{V12}, egr³/egr³; FRT^{82B}, scrib¹/FRT^{82B}, tub-gal80*. The haemolymph donors were: **E**, *w*. **F**, *w; egr³/egr³*. **G** and **H**, *w; UAS-RFP^{NLS}; hemesee-gal4*.